

A multicolor riboswitch-based platform for imaging of RNA in live mammalian cells

Esther Braselmann^{1,2}, Aleksandra J. Wierzbą^{3,7}, Jacob T. Polaski^{1,6,7}, Mikołaj Chromiński³, Zachariah E. Holmes¹, Sheng-Ting Hung⁴, Dilara Batan^{1,2}, Joshua R Wheeler¹, Roy Parker^{1,5}, Ralph Jimenez^{1,4}, Dorota Gryko³, Robert T. Batey¹ and Amy E. Palmer^{1,2*}

RNAs directly regulate a vast array of cellular processes, emphasizing the need for robust approaches to fluorescently label and track RNAs in living cells. Here, we develop an RNA imaging platform using the cobalamin riboswitch as an RNA tag and a series of probes containing cobalamin as a fluorescence quencher. This highly modular 'Riboglow' platform leverages different colored fluorescent dyes, linkers and riboswitch RNA tags to elicit fluorescence turn-on upon binding RNA. We demonstrate the ability of two different Riboglow probes to track mRNA and small noncoding RNA in live mammalian cells. A side-by-side comparison revealed that Riboglow outperformed the dye-binding aptamer Broccoli and performed on par with the gold standard RNA imaging system, the MS2-fluorescent protein system, while featuring a much smaller RNA tag. Together, the versatility of the Riboglow platform and ability to track diverse RNAs suggest broad applicability for a variety of imaging approaches.

The complex spatiotemporal dynamics of messenger RNAs (mRNAs) and noncoding RNAs (ncRNAs) affect virtually all aspects of cellular function. RNAs associate with a large group of RNA-binding proteins that dynamically modulate RNA localization and function¹. Such RNA–protein interactions govern mRNA processing, export from the nucleus, and assembly into translationally competent messages, as well as association into large macromolecular granules that are not translationally active, including processing bodies (P-bodies) and stress granules (SGs)^{2,3}. Similarly, uridine-rich small nuclear RNAs (U snRNAs, the RNA components of the spliceosome) dynamically associate with protein components to comprise the functional spliceosomal complex in the nucleus⁴. During stress, such as nutrient deprivation or bacterial infection, U snRNAs along with the splicing machinery can be transiently sequestered in cytosolic foci called U-bodies⁵. Given the intricate connection between RNA localization, dynamics and function, there has been a strong push to develop tools for visualization of RNA in live cells to elucidate mechanisms underlying dynamics of the mRNA and ncRNA life cycle.

Although there is a broad spectrum of tools for fluorescently tagging proteins in live cells, fewer approaches for live cell imaging of RNA exist. The most common system employs multimer RNA tags that bind an RNA-binding protein (MS2 or PP7 coat protein) fused to a fluorescent protein (FP)^{6,7}. The tag is genetically fused to an RNA of interest, and binding of MS2-FP concentrates the fluorescence signal on the RNA. One limitation of this approach is that many copies of the MS2 RNA tag are required to enhance fluorescence contrast, and the large size of the RNA tag bound to MS2-FP complexes (Supplementary Table 1) can perturb localization, dynamics and processing^{8,9} of the RNA. Still, this system is the gold standard in live cell RNA imaging, as it has been used successfully to interrogate mRNA dynamics over time at the single-molecule

level^{6,10,11}. An alternative approach involves fluorogenic dye-binding aptamers that give rise to a turn-on fluorescence signal when the dye binds the aptamer^{12–16}. Though numerous proof-of-principle aptamers have been developed, only the Spinach¹⁷, Broccoli¹⁸ and Mango^{19,20} aptamers have been used in live mammalian cells. These dye-binding aptamers have been used to visualize highly expressed RNA polymerase III-dependent transcripts such as 5S and U6 RNA^{20–22}. However, there are no reports of dye-binding aptamers being used to detect RNA polymerase II-dependent transcripts such as mRNAs, snRNAs, or microRNAs.

Here, we introduce a new approach for fluorescent tagging of RNA in live cells using a bacterial riboswitch as the RNA tag and a series of small molecular probes that undergo fluorescence turn-on upon binding the RNA tag. We took advantage of the robust folding of bacterial riboswitches in different genetic contexts in cells^{23,24}, while exploiting specific binding of the riboswitch RNA to its natural ligand, cobalamin (Cbl (1))²⁵. Cbl is an efficient fluorescence quencher when covalently coupled to a synthetic fluorophore^{26–28}. We developed a series of Cbl-fluorophore probes that result in fluorescence turn-on upon binding of Cbl to the RNA tag (Fig. 1a) and demonstrate the ability of this system to track recruitment of mRNA to stress granules and the small noncoding U1 RNA to cytosolic U-bodies in live mammalian cells.

Results

Design of Cbl-fluorophore probes. The Cbl riboswitch consists of the aptamer (Cbl-binding domain) and expression platform. Variants of both the full-length riboswitch sequence and the shorter aptamer domain were used (Supplementary Fig. 1; Supplementary Table 2), collectively referred to as the 'riboswitch RNA tag' in this study. The crystal structure of Cbl bound to the aptamer revealed that the Cbl 5'-hydroxyl group is accessible in the RNA-bound

¹Department of Chemistry and Biochemistry, University of Colorado Boulder, Boulder, CO, USA. ²BioFrontiers Institute, University of Colorado Boulder, Boulder, CO, USA. ³Institute of Organic Chemistry, Polish Academy of Sciences, Warsaw, Poland. ⁴JILA, University of Colorado and NIST, Boulder, CO, USA. ⁵Howard Hughes Medical Institute, Chevy Chase, MD, USA. ⁶Present address: Computational Biology Program, Public Health Sciences Division, Basic Sciences Division, Fred Hutchinson Cancer Research Center, Seattle, WA, USA. ⁷These authors contributed equally: Aleksandra J. Wierzbą, Jacob T. Polaski. *e-mail: amy.palmer@colorado.edu

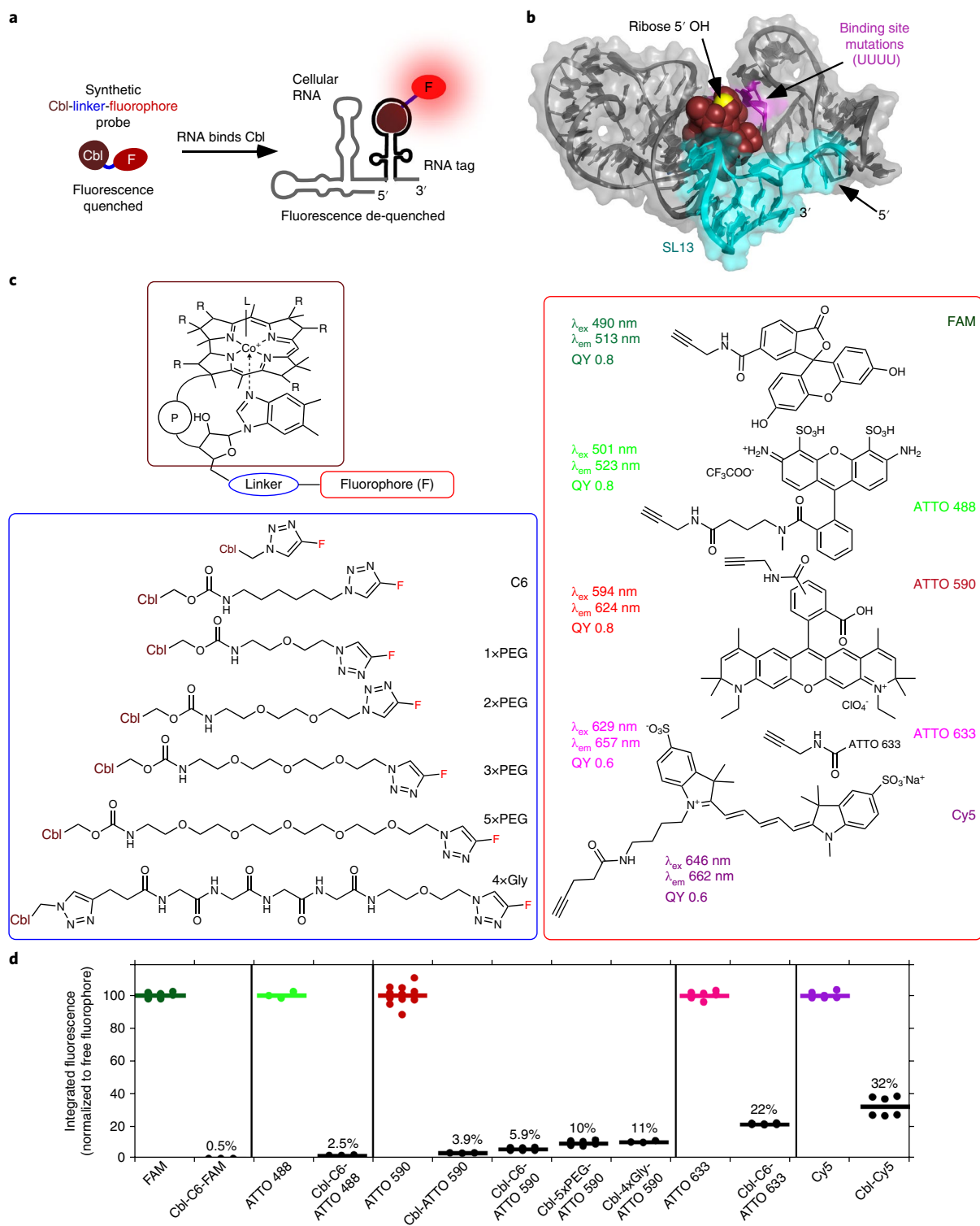


Fig. 1 | Covalent attachment of fluorophores to cobalamin (Cbl) results in fluorescence quenching, inducing fluorescence turn-on of the probe upon binding to riboswitch RNA. **a**, Principle of RNA-induced fluorescence turn-on for Cbl-fluorophore probes. Cbl (brown) acts as a quencher for the covalently attached fluorophore (F, red) owing to proximity. Upon RNA binding, Cbl is sterically separated from the fluorophore, resulting in de-quenching and fluorescence turn-on. **b**, Structure of Cbl riboswitch RNA (variant A) bound to Cbl²⁵. Stem-loop 13 (SL13, teal) is at the 3' end. Cbl is shown in brown spheres and the 5'-hydroxyl residue at the ribose moiety in yellow. Four bases that were mutated to UUUU to abolish binding to Cbl in variant A_{TMUT} are shown in magenta. **c**, Synthetic Cbl-fluorophore probes. The organic linker was attached at the 5'-hydroxyl of the ribose and conjugated to alkyne variants of commercially available fluorophores via click chemistry, resulting in the triazole linkage between linker and fluorophore. Note that ATTO 590 is a mixture of *para* and *meta* isomers and the structure of ATTO 633 is proprietary. L, cyano group, R, amide group. **d**, Comparison of the fluorescence intensities of the fluorophore and the Cbl-fluorophore probes. Fluorescence spectra of 5 μ M free fluorophores or Cbl-fluorophore probes were collected, the integrated intensity for each free fluorophore was set to 100% and the value for the Cbl-fluorophore probe was normalized relative to that of the corresponding fluorophore. Data are the mean for $n = 6, 6, 3, 3, 12, 3, 9, 6, 3, 6, 6, 6$ (datasets from left to right) independent measurements.

state²⁵ (Fig. 1b), prompting us to use this site for fluorophore conjugation via a copper catalyzed alkyne-azide cycloaddition reaction^{29,30} (Fig. 1c).

To assess how different fluorophores affect quenching, we synthesized a series of probes with different fluorophores conjugated to Cbl via a 6-carbon chain (C6) (Supplementary Note 1; Supplementary Fig. 2). The fluorescence of each probe was measured and compared to that of the free fluorophore (Fig. 1d). Cbl-C6-FAM (2) and Cbl-C6-ATTO 488 (3) retained only 0.5% and 2.5% fluorescence, respectively, indicating that quenching was highly efficient for probes with green fluorophores. In contrast, red and far-red probes retained more fluorescence (5.9% for Cbl-C6-ATTO 590 (4), 22% for Cbl-C6-ATTO 633 (5) and 32% for Cbl-Cy5 (6)), corresponding to moderate quenching (Fig. 1d). These results reveal a correlation between quenching efficiency and the excitation and emission wavelengths of the fluorophore.

By systematically varying the length of the chemical linker, we found that increasing linker length reduces quenching efficiency, consistent with observations in the literature²⁶. Addition of a C6 linker (~10.5 Å; length estimates in Supplementary Table 3) between Cbl and ATTO 590 resulted in higher residual fluorescence (5.9% for Cbl-C6-ATTO 590 vs. 3.9% for Cbl-ATTO 590 (7); Fig. 1d). Increasing the linker further to five polyethylene glycol (PEG) units (~17.5 Å) or a 4×glycine linker (~21.4 Å) increased the residual fluorescence to 10% and 11%, respectively. Similar trends were observed for probes with FAM as the fluorophore (Supplementary Fig. 3), confirming that quenching is most efficient when the fluorophore is close to Cbl.

RNA binding induces fluorescence turn-on. To test whether binding of Cbl to the riboswitch would sterically separate the fluorophore and quencher, resulting in fluorescence turn-on, we measured the fluorescence signal of Cbl-fluorophore probes in the presence and absence of a series of riboswitch variants. An increase in fluorescence was observed for all probes upon binding to Cbl riboswitches (Fig. 2), including the short riboswitch aptamer, A_T, the full-length riboswitch A, which contains an additional structural element to increase bulkiness, and variants B, C and D with different predicted secondary structures (Fig. 2a–c; Supplementary Fig. 4; see Supplementary Table 4 for a summary of fold turn-on results). Importantly, the fluorescence was not significantly changed in the presence of the negative control RNA A_{T,MUT}, which harbors four point mutations to abolish binding to Cbl, and RNA A_T did not affect the fluorescence signal of the free fluorophore (Supplementary Fig. 5). Combined, these results suggest that increasing steric bulk of the RNA can lead to increased fluorescence turn-on.

Because fluorophore spectral properties impacted the extent of quenching and fluorescence turn-on, we evaluated whether Förster resonance energy transfer (FRET) contributes to quenching by calculating the Förster radius R_0 and estimating the distance between the fluorophore and quencher (Supplementary Tables 3, 5 and 6). The estimated quencher–fluorophore distance for green fluorescent probes (FAM and ATTO 488) is significantly below the calculated R_0 value, consistent with efficient quenching (<3% residual fluorescence, Fig. 1d; Supplementary Table 5). For these probes, the bulkiest RNAs tested resulted in a fluorescence signal <6% of that of the free fluorophore (Fig. 2a), presumably because the length of the linker does not allow separation of fluorophore and quencher beyond R_0 . Though our theoretical estimates are consistent with a model in which FRET contributes to quenching, conjugates in the far-red wavelength regime (λ_{em} ~660 nm) lack spectral overlap with the Cbl absorbance spectrum (Supplementary Fig. 6) yet still exhibit moderate quenching, suggesting that non-FRET mechanisms such as contact quenching or electron transfer must also contribute. Probes with the ATTO 590 fluorophore have a Förster radius (R_0 = 20 Å) close to the estimated distance between the corrin ring

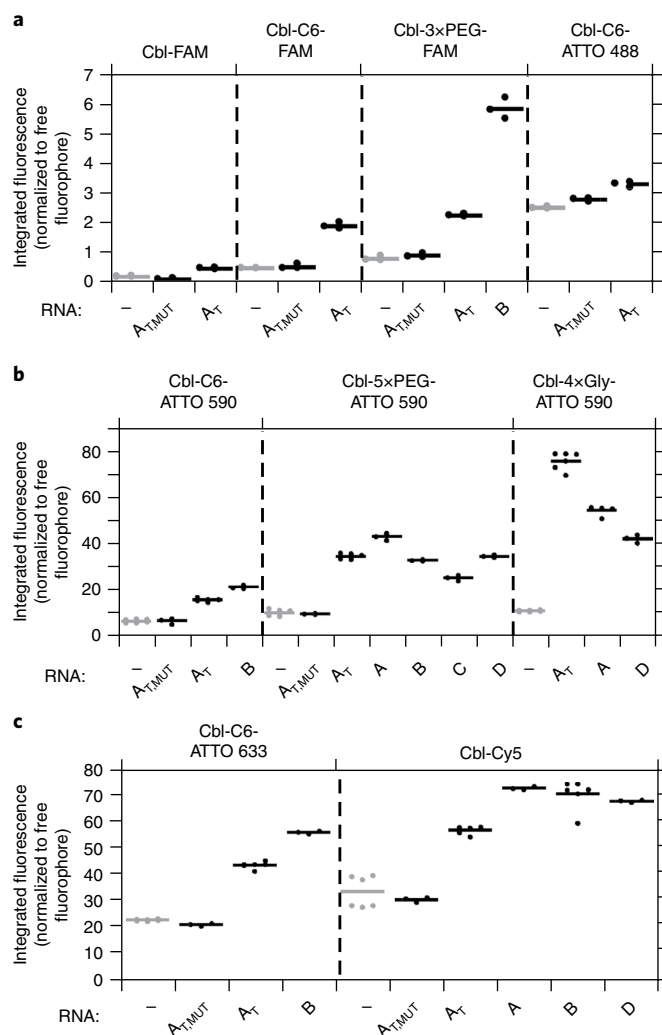


Fig. 2 | Cbl riboswitch RNAs induce fluorescence turn-on in Cbl-fluorophore probes in vitro. The fluorescence intensity of Cbl-fluorophore probes in the presence or absence of different RNAs was quantified as in Fig. 1d and normalized relative to the intensity of the free fluorophore. RNAs A, B, C and D are variants of Cbl-binding riboswitch sequences, where A_T refers to a truncated version of A with linker region J1/13 and stem-loop SL13 deleted (see also Fig. 1b). A_{T,MUT} contains four point mutations in the Cbl-binding site (see Fig. 1b for the position of these residues). **a**, Probes with fluorescence in the green wavelength range ($n=3$ independent measurements). **b**, Probes with fluorescence in the red wavelength range (from left to right, $n=9, 3, 6, 3, 6, 3, 3, 3, 3, 12, 6, 6$ and 3 independent measurements). **c**, Probes with fluorescence in the far-red wavelength range (from left to right, $n=6, 3, 6, 3, 6, 3, 6, 3, 6$ and 3). See Supplementary Table 4 for a summary.

and fluorophore (Supplementary Table 5), suggesting that these probes are particularly susceptible to large fluctuations in fluorescence intensity for small distance changes.

Biophysical characterization of RNA–probe complexes. We next identified RNA and Cbl-fluorophore probes with ideal photophysical behavior for cellular imaging and characterized their biophysical properties. We reasoned that shorter RNA tags would be less disruptive in RNA fusions. Therefore, we chose RNAs A and A_T for their small size (103 and 81 nucleotides, respectively) and induction of strong fluorescence turn-on in vitro (4.9× for A with Cbl-5×-PEG-ATTO 590 (8) and 7.3× for A_T with Cbl-4×Gly-ATTO 590

(9); Supplementary Table 4). We also included RNA D (130 nucleotides), because preliminary studies indicated high binding affinity to Cbl. Indeed, RNA tags A and D bind Cbl-5 \times -PEG-ATTO 590 tightly with dissociation constants (K_D) of 34 nM and 3 nM, respectively, comparable to the K_D for Cbl alone (Supplementary Fig. 7; Supplementary Table 7). The truncated riboswitch A_T bound Cbl-5 \times -PEG-ATTO590 with a lower affinity with a K_D of 1.3 μ M.

We chose Cbl-fluorophore probes with red and far-red fluorescent properties for further characterization because of the decreased cellular autofluorescence in this wavelength regime. Additionally, although green fluorescent probes display efficient quenching and reasonable fluorescence turn-on (up to 7.4 \times fluorescence turn-on for Cbl-3 \times -PEG-FAM (10) with B), the fluorescence signal after turn-on was low (only ~5% of fluorescence of free FAM (11)), raising concerns about the total signal intensity in microscopy applications. Therefore, red and far-red probes (Cbl-5 \times -PEG-ATTO 590, Cbl-4 \times Gly-ATTO 590 and Cbl-Cy5) were selected for cellular studies because they exhibited robust turn-on and a fluorescence signal closer to that of the free dye (Fig. 2b,c).

The quantum yield of Cbl-5 \times -PEG-ATTO590, Cbl-4 \times Gly-ATTO 590 and Cbl-Cy5 was determined in the presence and absence of A and D (Supplementary Fig. 8; Supplementary Table 8). We observed a decrease in quantum yield for Cbl-fluorophore probes compared to the free fluorophores and an increase in the presence of RNA, consistent with results from our plate reader fluorescence assay (Fig. 2b,c). Similarly, the fluorescence lifetime was reduced for Cbl-fluorophore probes compared to that of the free fluorophore and increased in the presence of the RNA (Supplementary Fig. 9; Supplementary Table 9). Lastly, we assessed photostability of the red Cbl-5 \times -PEG-ATTO 590 and the far-red Cbl-Cy5 bound to RNA A in vitro under constant illumination. As seen by others²², DFHBI-1T-Broc coli photobleached to <20% fluorescence within a second. In contrast, Cbl-Cy5 bound to A retained >80% fluorescence even after 50 s constant illumination (>60% fluorescence after 50 s for Cbl-5 \times -PEG-ATTO 590 bound to A; Supplementary Fig. 10; Supplementary Table 10). Together, tight binding of our probes to riboswitch variants A and D, robust increase in quantum yield upon RNA binding, as well as substantially slower photobleaching compared to the dye-binding aptamer Broccoli indicate favorable properties for cellular imaging applications.

Visualization of mRNA dynamics in live mammalian cells.

We tested our new RNA imaging platform by visualizing recruitment of β -actin mRNA (encoded by *ACTB*) to SGs in U2-OS cells tagged with the riboswitch variants (Fig. 3; Supplementary Fig. 11). In vitro-evolved dye-binding aptamers contain a G-quadruplex fold^{31,32}, which has been shown to complicate RNA folding in mammalian cells³³. A scaffold to improve folding in mammalian cells is often included for evolved aptamers when fused to mammalian RNAs^{20–22}, yet certain scaffolds increase undesired RNA processing in mammalian cells³⁴. Our RNA tag did not require the tRNA folding scaffold³⁵, and exclusion of the scaffold prevented unwanted processing (Supplementary Fig. 12) and reduced the overall tag size, prompting us to omit this scaffold for all further live-cell experiments. The residual unquenched fluorescence of the three Cbl-fluorophore probes used in cellular studies (Cbl-5 \times -PEG-ATTO 590, Cbl-4 \times Gly-ATTO 590 and Cbl-Cy5) revealed that in the absence of the riboswitch RNA, bead loading^{36–38} the probes in U2-OS cells gave rise to diffuse cytosolic and nuclear localization (Supplementary Fig. 13a–c). Treatment of U2-OS cells with arsenite induces formation of SGs that contain the marker protein G3BP1 (refs 39,40), tagged with GFP or the Halo-tag for labeling with red or far-red fluorophores JF585, SiR594 or JF646 (ref. 41; Supplementary Fig. 14; Fig. 3a). *ACTB* mRNA tagged with A localized to G3BP1-positive SGs^{39,40} via fluorescence in situ hybridization (FISH) in fixed cells (Supplementary Fig. 15a), similarly to endogenous *ACTB*

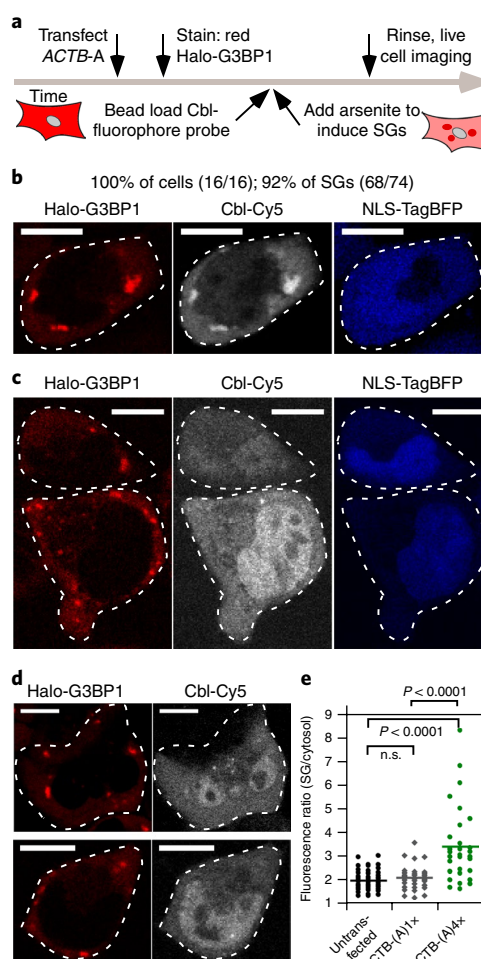


Fig. 3 | Monitoring *ACTB* mRNA localization to stress granules (SG) via Cbl-fluorophore probe binding to the RNA tag A. **a**, Experimental strategy for labeling the Halo-tagged G3BP1 SG marker protein with the red fluorescent JF585 dye, followed by bead loading the Cbl-fluorophore probe, induction of SGs by arsenite for 30–45 min and live cell imaging. **b**, U2-OS cells producing Halo-G3BP1 were transfected with *ACTB*-(A)_{4x} and the transfection marker TagBFP. 24 h post-transfection, cells were stained with the JF585 Halo dye. Shown is a representative live cell to assess colocalization of the SG marker protein Halo-G3BP1 and *ACTB* mRNA (3 independent experiments; 16 cells; 74 SGs). At least one SG was visible in all 16 cells (100%), and 92% of SGs were detectable. **c**, The same experiment as in **b** was performed, except that *ACTB*-(A)_{1x} was transfected (3 independent experiments; 14 cells; 30 SGs). Two representative live cells are presented. In 43% of the cells at least one SG was detectable and 40% of all SGs were detected in the Cbl-Cy5 channel. **d**, The same experiment as in **b** was performed, except that *ACTB*-(A)_{4x} was not transfected (2 independent experiments; 39 cells; 100 SGs). Two representative live cells are presented. In 38% of the cells, at least one SG was detectable, and 32% of all SGs were visible in the Cbl-Cy5 channel. **e**, Quantification of fluorescence signal accumulation in representative SGs (line represents mean). Scale bars, 10 μ m. One-way ANOVA (95% confidence limit); post hoc test (Tukey HSD). n.s., not significant.

mRNA (Supplementary Fig. 16). A transfection marker was used to identify cells containing A-tagged *ACTB* mRNA (Supplementary Fig. 17); Cbl-Cy5 probe was loaded in live cells, and SGs were induced by arsenite (Fig. 3a). We observed robust accumulation of Cbl-Cy5 fluorescence in SGs upon arsenite treatment when four copies of A were used, but not when only one copy was used (Fig. 3b,c; Supplementary Fig. 18). Similar results were obtained

with the Cbl-4xGly-ATTO 590 probe (Supplementary Fig. 19). Finally, time-lapse imaging enabled detection of the formation of ACTB-(A)4x mRNA-containing SGs and tracking of SG dynamics for ~50 min (Supplementary Fig. 20). These experiments demonstrate that ACTB mRNA recruitment to SGs and mRNA dynamics over time can be visualized via the riboswitch tag.

The Cbl-Cy5 fluorescence signal remained diffuse throughout the cytosol in untransfected cells even when G3BP1-labeled SGs were induced (Fig. 3d), indicating that Cbl-Cy5 specifically binds to the A aptamer. In the absence of arsenite stress, a very small fraction of transfected cells showed SG formation, whereby Cbl-Cy5 fluorescence localized to SGs (Supplementary Fig. 21). In this case, the SGs result from the process of transfection, which has been shown to induce SGs occasionally⁴². The expression level of mRNA fusions and probe uptake efficiency (Supplementary Fig. 13a) are heterogeneous, which may explain the broad distribution of Cbl-Cy5 fluorescence increase in SGs (Fig. 3e). To directly confirm accumulation of tagged ACTB mRNA in SGs, we correlated the live cell mRNA signal with FISH on the same cells after fixation (Supplementary Fig. 22). In summary, we demonstrated recruitment of ACTB mRNA to SGs in live cells using our riboswitch tagging system, enabling visualization of 100% cells containing at least 1 SG and 92% of all SGs for the Cbl-Cy5 probe, with the additional benefit of allowing visualization with two orthogonal colors (ATTO 590 and Cy5).

Comparison with Broccoli and MS2. We next compared our riboswitch-based RNA tag with commonly used RNA imaging platforms, namely the dye-binding aptamer Broccoli^{17,21} and the MS2 system^{6,43}, using recruitment of tagged ACTB mRNA to SGs as a model system. ACTB mRNA was tagged with a dimer of Broccoli dimers integrated in the F30 folding scaffold²¹ such that each tag binds four fluorogens (called 2x dBroccoli) or 1, 2, 4 or 24 copies of the MS2 stem-loop (SL) repeat (Supplementary Fig. 11; Supplementary Table 1). Because each MS2-SL binds a dimer of MS2-GFP⁴⁴, we chose ACTB-(MS2-SL)2x to compare to our platform in which four copies of the RNA tag were used (Supplementary Table 1). Tagging of ACTB mRNA with 2x dBroccoli or with up to 24 copies of the MS2-SL does not affect ACTB mRNA localization to SGs (Supplementary Fig. 15b,c).

Before assessing ACTB mRNA recruitment to SGs using the 2x dBroccoli tag, we confirmed that we could visualize Broccoli-tagged 5S and U6 RNA using recommended experimental procedures²¹ (Supplementary Fig. 23). We then examined mRNA recruitment to SGs and found that in 90% of transfected cells containing SGs in the red fluorescent (Halo-G3BP1) channel, no corresponding SGs in the green Broccoli channel were detectable (401/445 cells; Fig. 4a; Supplementary Fig. 24). In the remaining 10% of cells, green puncta colocalizing with Halo-G3BP1-positive SGs were detectable, but only a minor fraction of all SGs were detected (4% of SG; 64/1,790 SGs in total). As seen for tagging with the riboswitch, transient transfection occasionally induced G3BP1-positive SGs even in the absence of arsenite treatment (Supplementary Fig. 25). While rapid photobleaching of Broccoli is a well-established complication of the Spinach and Broccoli system^{22,45} (Supplementary Fig. 10), we used laser scanning confocal microscopy, a modality that resembles pulsed illumination that is shown to be ideal for imaging Spinach and Broccoli⁴⁵. Nonetheless, we were unable to robustly visualize recruitment of ACTB mRNA tagged with a total of four Broccoli copies to SGs.

To evaluate the MS2 system, we assessed ACTB mRNA recruitment to SGs tagged with 1, 2, 4 or 24 copies of MS2-SL (Supplementary Fig. 26; Fig. 4b). These experiments were performed in a variant of the U2-OS Halo-G3BP1 in which NLS-MS2-GFP was also stably produced from the chromosome, such that MS2-GFP remains nuclear in the absence of ACTB mRNA fused to MS2-SL (Supplementary Fig. 27). Localization of mRNA tagged

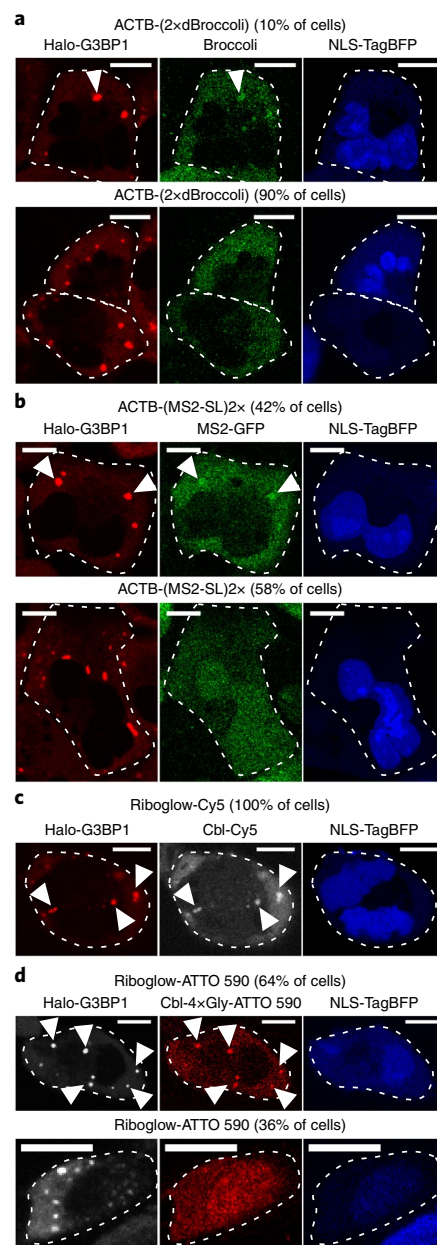


Fig. 4 | Comparison of ACTB mRNA imaging in stress granules (SG) by RNA tagging systems with four fluorophores per RNA. A plasmid encoding tagged ACTB was transfected into U2-OS Halo-G3BP1 cells with the NLS-TagBFP transfection marker. Halo-G3BP1 was labeled with a Halo dye for SG identification, and SGs were induced by arsenite. **a**, ACTB-(2x dBroccoli) was transfected and the Broccoli probe DFHBI-1T was added; cells were assessed for SGs in the green channel (445 cells; 3 independent experiments). In 10% of all transfected cells at least one SG was detected, and 4% of all SGs were detected (1,790 SGs, 445 cells). **b**, ACTB fused with two MS2-SL repeats was transfected with NLS-TagBFP into U2-OS Halo-G3BP1 cells that stably produce MS2-GFP (in 42% of all transfected cells at least one SG was detected, and 17% of all SGs were detected; 162 SGs total in 53 cells; 2 independent experiments). **c**, **d**, ACTB tagged with four copies of the riboswitch tag A was transfected with NLS-TagBFP in U2-OS Halo-G3BP1 cells. **c**, Cbl-Cy5 was loaded in cells (in 100% of all transfected cells at least one SG was detected in the Cy5 channel, and 92% of all SGs were detected; 74 SGs total in 16 cells, 3 independent experiments). **d**, Cbl-ATTO 590 was loaded in cells (in 64% of all transfected cells at least one SG was detected in the Cy5 channel, and 58% of all SGs were detected; 59 SGs total in 22 cells; 2 independent experiments). Scale bars, 10 μ m. White arrowheads indicate SGs.

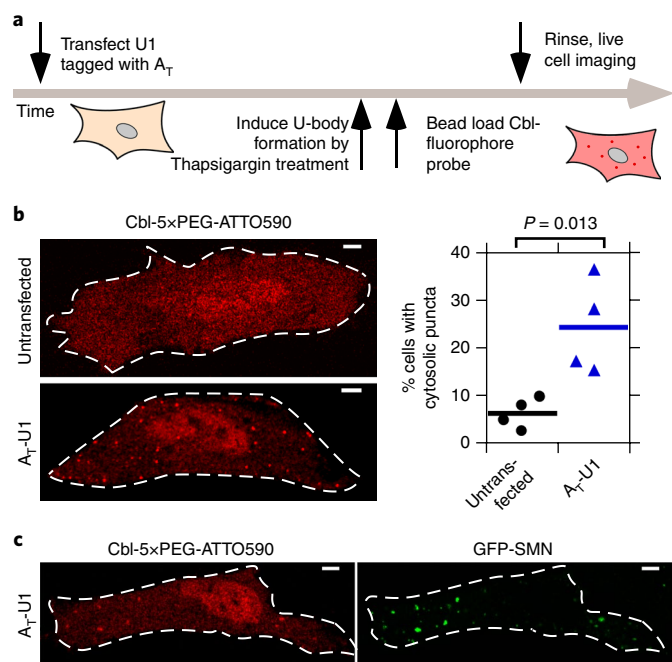


Fig. 5 | Monitoring cytosolic U-bodies via A_T -tagged U1. **a**, After transient transfection of A_T -U1, U-bodies were induced by thapsigargin treatment and imaged by live cell microscopy. **b**, Cbl-5xPEG-ATTO 590 localization to cytosolic puncta in thapsigargin-treated HeLa cells was more likely when A_T -U1 was transfected (A_T -U1, mean from 4 independent experiments using 326 cells; untransfected, mean from 4 independent experiments using 677 cells). One-way ANOVA (95% confidence limit); post hoc test (Tukey HSD). **c**, Cytosolic puncta in thapsigargin-treated cells producing A_T -U1 RNA colocalize to GFP-SMN U-bodies. 3 independent experiments, 10 cells. Scale bars, 5 μ m.

with 24x MS2-SL to SGs was readily visualized via recruitment of MS2-GFP to SGs in the majority of transfected cells containing SGs (86%, 43/50 cells; Supplementary Fig. 26d). With one, two or four copies of MS2-SL, visualization of ACTB mRNA localization to SGs was less efficient (28% of cells, 26% of all SGs for 1x MS2-SL tag; 42% of cells, 17% of all SGs for 2x MS2-SL tag; 45% of cells, 28% of all SGs for 4x MS2-SL tag, Fig. 4b; Supplementary Fig. 26). The fluorescence contrast for SGs over cytosolic background signal was markedly reduced for 1x, 2x, or 4x-MS2-SL compared to 24x MS2-SL (Supplementary Fig. 26). In summary, our riboswitch tagging system performed similarly to the 24x MS2 system with respect to reliably detecting localization of a candidate mRNA (ACTB) to SGs (Fig. 4c,d), and our platform outperforms both the Broccoli and MS2 system on a fluorophore-by-fluorophore basis (Fig. 4).

Sequestration of U1 snRNA in U-bodies in live cells. The small size of our truncated RNA tag (A_T , 81 nucleotides (nt)) opens up the possibility for tagging ncRNAs such as snRNA U1 in live cells. Proper processing of U snRNA depends on its length with an overall size limit of 200–300 nt⁴⁶, limiting the size of any U1 fusion tag to ~100 nt. We introduced one copy of A_T (81 nt) near the 5' end of the U1 coding sequence (Supplementary Fig. 11), a position previously shown to be compatible with short RNA tags⁴⁷. A_T -tagged U1 colocalized with the Cajal body marker protein coilin in the nucleus of HeLa cells (Supplementary Fig. 28a,b), consistent with previously observed U snRNAs localization⁴⁸. Treatment of HeLa cells with thapsigargin induced sequestration of endogenous U1 snRNA and A_T -tagged U1 in cytosolic U-bodies containing the marker proteins DEAD-Box Helicase 20 (DDX20) and survival motor neuron (SMN) (Supplementary Figs. 28c and 29). When

we loaded Cbl-fluorophore probes in live HeLa cells, nonspecific puncta formation was observed for Cbl-Cy5 and for Cbl-4xGly-ATTO 590, but not for Cbl-5xPEG-ATTO 590, even at elevated probe concentrations (Supplementary Fig. 13d–g), leading us to choose Cbl-5xPEG-ATTO 590 for live U1 snRNA visualization. After thapsigargin treatment of cells transiently transfected with A_T -tagged U1 (Fig. 5a), 24 ± 10% of cells contained cytosolic puncta resembling U-bodies, whereas such puncta were only observed in 6 ± 3% of untransfected cells (Fig. 5b), consistent with previous studies in which ~25% of HeLa cells contained U-bodies upon thapsigargin-treatment⁵. No cytosolic puncta were observed in the absence of thapsigargin treatment (Supplementary Fig. 30). Finally, co-transfection of a plasmid encoding GFP-SMN together with a plasmid encoding A_T -tagged U1 confirmed colocalization of SMN and U1 (Fig. 5c; Supplementary Fig. 31). Together, we conclude that our riboswitch-based imaging system allows live cell visualization of small noncoding RNAs such as the snRNA U1.

Discussion

In this work we introduce a new riboswitch-based RNA imaging platform that we call 'Riboglow', characterized by several features that distinguish it from previous RNA-detection systems. First, the RNA tag is small and exploits the selective and high-affinity (K_D in the nanomolar range) binding between a riboswitch and its cognate ligand Cbl. Second, because the RNA tag binds the fluorescence quencher Cbl, the system is compatible with a wide range of synthetic fluorophores spanning the green-to-far-red spectral range. The Riboglow-ATTO 590 and Riboglow-Cy5 probes used for live cell studies retain favorable photophysical properties of the parent dyes, including slow photobleaching, when bound to RNA. Indeed, we were able to visualize tagged mRNA over 50 min without detectable photobleaching (Supplementary Fig. 20). Third, our RNA tag is not subjected to undesired processing and hence does not require the tRNA-like scaffold used for other dye-binding aptamers. Fourth, Cbl riboswitches include a large family of RNA sequences that all bind Cbl⁴⁹ that can be exploited for future optimization and customization of the Riboglow platform. Fifth, the fluorescence lifetime of ATTO 590 and Cy5 in the context of our probes varies when the RNA binds (Supplementary Fig. 9), raising the possibility of using this system for fluorescence lifetime imaging. Finally, and perhaps most importantly, we were able to visualize recruitment of RNA polymerase II-dependent transcripts (mRNA and snRNA) to RNA-protein granules, whereby the short size of the RNA tag (~80 nt for RNA tag A_T) enabled tagging and visualization of U1 snRNA in live cells for the first time.

To compare the performance of Riboglow to those of existing RNA imaging platforms, we characterized recruitment of mRNA to SGs in live cells. Riboglow is most similar to dye-binding systems (Spinach¹⁷, Broccoli¹⁸ and Mango^{19,20}) in terms of concept, size of the RNA tag, and molar mass of the probe. We used a two-fold repeat of dimer-Broccoli because it is the brightest of the Spinach/Broccoli family and is the most widely used of the dye-binding aptamers. Compared to Riboglow, a small minority of SGs were detected via the Broccoli-labeled mRNA (4% of SGs versus 92% for Riboglow-Cy5 or 58% of SGs for Riboglow-ATTO 590). This is perhaps not surprising, because dye-binding aptamers have not yet been used to detect RNA polymerase II transcripts such as mRNA. Rather, these systems have been applied to RNA polymerase III transcripts^{20,22}, which are expressed at higher levels, particularly in HEK 293 cells. It is noteworthy that Riboglow displays a much weaker fold fluorescence turn-on in vitro compared to the ~1,000-fold in vitro fluorescence enhancement for both Broccoli¹⁸ and Mango^{19,20}. However, cellular contrast defined as fluorescence signal in RNA-granules versus cytosolic background was comparable in our platform (~3–4-fold, Fig. 3d) and in Mango-tagged 5S-RNA and U6-RNA foci (~2–3-fold fluorescence turn-on in fixed

mammalian cells²⁰). The in vitro-evolved dye-binding aptamers all feature G-quadruplex RNA folds^{32,33}, and it has been shown that the dyes can bind other G-quadruplex RNAs nonspecifically in cells³³, possibly contributing to diminished cellular contrast. Moreover, cellular contrast is influenced by folding of the RNA tag in the cellular environment, temperature- and salt-dependent stability of the RNA–probe complex, and probe photobleaching properties.

The MS2/PP7 system is the gold standard for detection of mRNA dynamics in mammalian cells^{6,7}. Indeed, we found that 1×, 2×, 4×, and 24× copies of the stem-loop all permitted visualization of mRNA recruitment to SGs. Not surprisingly, the 24× tag yielded the strongest fluorescence contrast and led to detection of the greatest number of SGs (76% of all SGs). Our Riboglow platform outperformed the MS2 system when the same number of fluorogens tagged the RNA (Fig. 4). Riboglow even compared favorably with the 24× MS2 system, yielding robust detection of SGs in transfected cells (92% of SGs for Riboglow-Cy5 and 58% of SGs for Riboglow-ATTO 590) and 3–4× fluorescence contrast of labeled mRNA in SGs.

There are some properties of Riboglow that are less favorable when compared to other RNA-tagging systems. Though the Broccoli probe DFHBI-1T and Mango probe TO1-biotin are cell permeable, we use bead loading for cellular Cbl-fluorophore probe uptake. Although we have found bead loading to be a robust and simple procedure that is routinely used in other live cell imaging applications^{36,37}, this process adds an additional step to the imaging process. Utilization of the natural Cbl uptake route may present an alternative in the future⁵⁰. Additionally, mammalian cells contain at least four known Cbl-binding proteins, and it is possible that our Cbl-fluorophore probes could bind to these proteins, yielding fluorescence turn-on (much like dyes binding to G-quadruplexes in cells³³). Although we observe robust 3–4× contrast when tracking recruitment of RNA to RNA–protein granules, if nonspecific binding is a problem for other applications, the Cbl-fluorophore probes could be further engineered to enhance specificity.

Overall, the Riboglow platform compares favorably in a direct side-by-side comparison with existing RNA imaging platforms and presents an orthogonal approach for live cell RNA imaging applications. The highly modular nature of the Riboglow platform currently allows a choice of imaging wavelength and detection of mRNAs as well as small noncoding RNAs while presenting a system that is ideally set up for straightforward future customization to include desired features for RNA imaging.

Methods

Methods, including statements of data availability and any associated accession codes and references, are available at <https://doi.org/10.1038/s41589-018-0103-7>.

Received: 16 May 2018; Accepted: 13 June 2018;
Published online: 30 July 2018

References

- Gerstberger, S., Hafner, M. & Tuschl, T. A census of human RNA-binding proteins. *Nat. Rev. Genet.* **15**, 829–845 (2014).
- Buchan, J. R. & Parker, R. Eukaryotic stress granules: the ins and outs of translation. *Mol. Cell* **36**, 932–941 (2009).
- Decker, C. J. & Parker, R. P-bodies and stress granules: possible roles in the control of translation and mRNA degradation. *Cold Spring Harb. Perspect. Biol.* **4**, a012286 (2012).
- Matera, A. G. & Wang, Z. A day in the life of the spliceosome. *Nat. Rev. Mol. Cell Biol.* **15**, 108–121 (2014).
- Tsalikis, J. et al. Intracellular bacterial pathogens trigger the formation of U small nuclear RNA bodies (U bodies) through metabolic stress induction. *J. Biol. Chem.* **290**, 20904–20918 (2015).
- Fusco, D. et al. Single mRNA molecules demonstrate probabilistic movement in living mammalian cells. *Curr. Biol.* **13**, 161–167 (2003).
- Wu, B., Chen, J. & Singer, R. H. Background free imaging of single mRNAs in live cells using split fluorescent proteins. *Sci. Rep.* **4**, 3615 (2014).
- Tutucci, E. et al. An improved MS2 system for accurate reporting of the mRNA life cycle. *Nat. Methods* **15**, 81–89 (2018).
- Garcia, J. F. & Parker, R. MS2 coat proteins bound to yeast mRNAs block 5' to 3' degradation and trap mRNA decay products: implications for the localization of mRNAs by MS2-MCP system. *RNA* **21**, 1393–1395 (2015).
- Wu, B., Eliscovich, C., Yoon, Y. J. & Singer, R. H. Translation dynamics of single mRNAs in live cells and neurons. *Science* **352**, 1430–1435 (2016).
- Katz, Z. B. et al. Mapping translation 'hot-spots' in live cells by tracking single molecules of mRNA and ribosomes. *eLife* **5**, 1–17 (2016).
- Nguyen, D. H., DeFina, S. C., Fink, W. H. & Dieckmann, T. Binding to an RNA aptamer changes the charge distribution and conformation of malachite green. *J. Am. Chem. Soc.* **124**, 15081–15084 (2002).
- Babendure, J. R., Adams, S. R. & Tsien, R. Y. Aptamers switch on fluorescence of triphenylmethane dyes. *J. Am. Chem. Soc.* **125**, 14716–14717 (2003).
- Arora, A., Sunbul, M. & Jäschke, A. Dual-colour imaging of RNAs using quencher- and fluorophore-binding aptamers. *Nucleic Acids Res.* **43**, e144 (2015).
- Sunbul, M. & Jäschke, A. Contact-mediated quenching for RNA imaging in bacteria with a fluorophore-binding aptamer. *Angew. Chem. Int. Edn. Engl.* **52**, 13401–13404 (2013).
- Tan, X. et al. Fluoromolecules consisting of a promiscuous RNA aptamer and red or blue fluorogenic cyanine dyes: selection, characterization, and bioimaging. *J. Am. Chem. Soc.* **139**, 9001–9009 (2017).
- Paige, J. S., Wu, K. Y. & Jaffrey, S. R. RNA mimics of green fluorescent protein. *Science* **333**, 642–646 (2011).
- Filonov, G. S., Moon, J. D., Svendsen, N. & Jaffrey, S. R. Broccoli: rapid selection of an RNA mimic of green fluorescent protein by fluorescence-based selection and directed evolution. *J. Am. Chem. Soc.* **136**, 16299–16308 (2014).
- Dolgosheina, E. V. et al. RNA mango aptamer-fluorophore: a bright, high-affinity complex for RNA labeling and tracking. *ACS Chem. Biol.* **9**, 2412–2420 (2014).
- Autour, A. et al. Fluorogenic RNA Mango aptamers for imaging small non-coding RNAs in mammalian cells. *Nat. Commun.* **9**, 656 (2018).
- Filonov, G. S. & Jaffrey, S. R. RNA imaging with dimeric Broccoli in live bacterial and mammalian cells. *Curr. Protoc. Chem. Biol.* **8**, 1–28 (2016).
- Song, W. et al. Imaging RNA polymerase III transcription using a photostable RNA-fluorophore complex. *Nat. Chem. Biol.* **13**, 1187–1194 (2017).
- Ceres, P., Trausch, J. J. & Batey, R. T. Engineering modular 'ON' RNA switches using biological components. *Nucleic Acids Res.* **41**, 10449–10461 (2013).
- Ceres, P., Garst, A. D., Marciano-Velázquez, J. G. & Batey, R. T. Modularity of select riboswitch expression platforms enables facile engineering of novel genetic regulatory devices. *ACS Synth. Biol.* **2**, 463–472 (2013).
- Johnson, J. E. Jr., Reyes, F. E., Polaski, J. T. & Batey, R. T. B12 cofactors directly stabilize an mRNA regulatory switch. *Nature* **492**, 133–137 (2012).
- Lee, M. & Grissom, C. B. Design, synthesis, and characterization of fluorescent cobalamin analogues with high quantum efficiencies. *Org. Lett.* **11**, 2499–2502 (2009).
- Smeltzer, C. C. et al. Synthesis and characterization of fluorescent cobalamin (CobalaFluor) derivatives for imaging. *Org. Lett.* **3**, 799–801 (2001).
- Fedosov, S. N. et al. Application of a fluorescent cobalamin analogue for analysis of the binding kinetics. A study employing recombinant human transcobalamin and intrinsic factor. *FEBS J.* **273**, 4742–4753 (2006).
- Chromiński, M. & Gryko, D. "Clickable" vitamin B12 derivative. *Chemistry* **19**, 5141–5148 (2013).
- Loska, R., Janiga, A. & Gryko, D. Design and synthesis of protoporphyrin IX/vitamin B-12 molecular hybrids via CuAAC reaction. *J. Porphy. Phtalocyanines* **17**, 104–117 (2013).
- Trachman, R. J. III et al. Structural basis for high-affinity fluorophore binding and activation by RNA Mango. *Nat. Chem. Biol.* **13**, 807–813 (2017).
- Warner, K. D. et al. Structural basis for activity of highly efficient RNA mimics of green fluorescent protein. *Nat. Struct. Mol. Biol.* **21**, 658–663 (2014).
- Jeng, S. C. Y., Chan, H. H. Y., Booy, E. P., McKenna, S. A. & Unrau, P. J. Fluorophore ligand binding and complex stabilization of the RNA Mango and RNA Spinach aptamers. *RNA* **22**, 1884–1892 (2016).
- Filonov, G. S., Kam, C. W., Song, W. & Jaffrey, S. R. In-gel imaging of RNA processing using broccoli reveals optimal aptamer expression strategies. *Chem. Biol.* **22**, 649–660 (2015).
- Ponchon, L. & Dardel, F. Recombinant RNA technology: the tRNA scaffold. *Nat. Methods* **4**, 571–576 (2007).
- Morisaki, T. et al. Real-time quantification of single RNA translation dynamics in living cells. *Science* **352**, 1425–1429 (2016).
- Hayashi-Takanaka, Y. et al. Tracking epigenetic histone modifications in single cells using Fab-based live endogenous modification labeling. *Nucleic Acids Res.* **39**, 6475–6488 (2011).
- McNeil, P. L. & Warder, E. Glass beads load macromolecules into living cells. *J. Cell Sci.* **88**, 669–678 (1987).
- Nelles, D. A. et al. Programmable RNA tracking in live cells with CRISPR/Cas9. *Cell* **165**, 488–496 (2016).

40. Zurla, C., Lifland, A. W. & Santangelo, P. J. Characterizing mRNA interactions with RNA granules during translation initiation inhibition. *PLoS One* **6**, e19727 (2011).
41. Grimm, J. B. et al. A general method to fine-tune fluorophores for live-cell and in vivo imaging. *Nat. Methods* **14**, 987–994 (2017).
42. Kedersha, N., Tisdale, S., Hickman, T. & Anderson, P. Real-time and quantitative imaging of mammalian stress granules and processing bodies. *Methods Enzymol.* **448**, 521–552 (2008).
43. Wu, B., Chao, J. A. & Singer, R. H. Fluorescence fluctuation spectroscopy enables quantitative imaging of single mRNAs in living cells. *Biophys. J.* **102**, 2936–2944 (2012).
44. Ni, C. Z. et al. Crystal structure of the MS2 coat protein dimer: implications for RNA binding and virus assembly. *Structure* **3**, 255–263 (1995).
45. Han, K. Y., Leslie, B. J., Fei, J., Zhang, J. & Ha, T. Understanding the photophysics of the spinach-DFHBI RNA aptamer-fluorogen complex to improve live-cell RNA imaging. *J. Am. Chem. Soc.* **135**, 19033–19038 (2013).
46. McCloskey, A., Taniguchi, I., Shinmyozu, K. & Ohno, M. hnRNP C tetramer measures RNA length to classify RNA polymerase II transcripts for export. *Science* **335**, 1643–1646 (2012).
47. Ishikawa, H. et al. Identification of truncated forms of U1 snRNA reveals a novel RNA degradation pathway during snRNP biogenesis. *Nucleic Acids Res.* **42**, 2708–2724 (2014).
48. Hutten, S., Chachami, G., Winter, U., Melchior, F. & Lamond, A. I. A role for the Cajal-body-associated SUMO isopeptidase USPL1 in snRNA transcription mediated by RNA polymerase II. *J. Cell Sci.* **127**, 1065–1078 (2014).
49. Nahvi, A., Barrick, J. E. & Breaker, R. R. Coenzyme B12 riboswitches are widespread genetic control elements in prokaryotes. *Nucleic Acids Res.* **32**, 143–150 (2004).
50. Quadros, E. V. & Sequeira, J. M. Cellular uptake of cobalamin: transcobalamin and the TCbIR/CD320 receptor. *Biochimie* **95**, 1008–1018 (2013).

Acknowledgements

The authors would like to acknowledge financial support from the Human Frontiers Science Project and NIH Director's Pioneer Award GM114863 (to A.E.P.). We acknowledge support from the National Science Centre, SYMFONIA DEC-2014/12/W/ST5/00589 to D. Gryko and A.J.W., the National Institutes of Health (5R01 GM073850)

to R.T.B., and NSF Physics Frontier Center at JILA (PHY1734006) to R.J. We thank L. Lavis (Janelia Research Campus) for providing fluorophores JF585, SiR594 and JF646 for Halo staining, S. Jaffrey (Cornell University) and G. Matera (UNC Chapel Hill) for contributing plasmids and S. Shukla and J. Garcia for helpful discussions; T. Stasevich, D. Muhlrad, J. Lee and M. Lo for technical expertise; and to J. Eberhard and J. Gassensmith for helpful discussions. The imaging work was performed at the BioFrontiers Institute Advanced Light Microscopy Core, whose Nikon A1R microscope was acquired by the generous support of the NIST-CU Cooperative Agreement award number 70NANB15H226. R.J. is a staff member in the Quantum Physics Division of the National Institute of Standards and Technology (NIST). Certain commercial equipment, instruments, or materials are identified in this paper in order to specify the experimental procedure adequately. Such identification is not intended to imply recommendation or endorsement by the NIST, nor is it intended to imply that the materials or equipment identified are necessarily the best available for the purpose.

Author contributions

E.B., J.T.P., R.T.B. and A.E.P. conceptualized and designed the study. J.T.P. and R.T.B. rationally designed riboswitch variants. E.B., J.T.P., R.T.B., A.J.W., D.G. and A.E.P. designed organic probes. A.J.W. and M.C. synthesized organic probes. J.T.P. and Z.E.H. purified riboswitch variants for in vitro work. E.B. performed in vitro work, designed and performed cellular work, and analyzed data with input from all authors. D.B. constructed plasmids and assisted with cellular work. S.-T.H. performed in vitro fluorescence lifetime and bleaching experiments. J.R.W. made the Halo-G3BP1 U2-OS cell line. R.P. and R.J. provided critical advice. E.B. and A.E.P. wrote the manuscript with edits from all authors.

Competing interests

The authors declare no competing interests.

Additional information

Supplementary information is available for this paper at <https://doi.org/10.1038/s41589-018-0103-7>.

Reprints and permissions information is available at www.nature.com/reprints.

Correspondence and requests for materials should be addressed to A.E.P.

Publisher's note: Springer Nature remains neutral with regard to jurisdictional claims in published maps and institutional affiliations.

Methods

Synthesis of fluorophore probes. Synthesis and characterization of probes are described in Supplementary Note 1. All probes are derivatives of CN-Cbl (Supplementary Fig. 2; see Supplementary Table 11 for photophysical properties).

RNA synthesis and preparation. For all in vitro experiments, DNA templates were amplified using recursive PCR and transcribed by T7 RNA polymerase using established methods^{51,52}. Transcription reactions were purified using the appropriate percentage denaturing polyacrylamide gel (8 M urea, 29:1 acrylamide:bisacrylamide) based on RNA length. Transcripts were visualized by UV shadowing, excised from the gel and soaked overnight in 0.5× TE buffer (10 mM Tris-HCl, pH 8.0 and 1 mM EDTA) at 4 °C. RNAs were buffer exchanged into 0.5× TE and concentrated using centrifugal concentrators (Amicon) with the appropriate molecular-weight cutoff. RNA concentration was determined using the absorbance at 260 nm and molar extinction coefficients calculated as the summation of the individual bases. Sequences and secondary structures of all riboswitch RNAs used in this study are shown in Supplementary Table 2 and Supplementary Fig. 1, and the published sequence for the Broccoli sequence was used (5'-GGA GCG CGG AGA CGG TCG GGT CCA GAT ATT CGT ATC TGT CGA GTA GAG TGT GGG CTC CGC GC)²¹.

Absorbance measurements and quantum yield determination. Absorbance spectra were collected using a Cary 500 UV-VIS-NIR spectrophotometer and buffer subtracted. The quantum yield (Q) of probes was determined by comparison with the published Q of ATTO 590 (0.80, Atto tec) or Cy5 (0.28, Lumiprobe). All experiments were done in RNA buffer (100 mM KCl, 10 mM NaCl, 1 mM MgCl₂, and 50 mM HEPES, pH 8.0). First, absorbance was determined at the excitation wavelength (Supplementary Table 11) for a dilution series of free fluorophore and Cbl-fluorophore probes with or without different RNAs. To ensure saturation of binding, the concentration was chosen such that the final concentration of RNA was above 5 μM in the most diluted sample. The fluorescence spectrum at the emission range (Supplementary Table 11) for each sample was then recorded using a PTI-fluorimeter (1 nm steps, 1 s integration time, 2 nm slits for the excitation and 4 nm slits for detector). After subtracting the buffer background signal, the fluorescence signal for each sample was integrated and plotted against the absorption. The steepness of the resulting linear plot for each dilution series reports on Q relative to the reference of the free fluorophore (Supplementary Table 8). These measurements were done once for the Q determination, and spectra were comparable with absorbance and fluorescence measurements done for fold fluorescence measurements.

Fluorescence lifetime measurements. The fluorescence lifetime of Cbl-fluorophore probes in the presence and absence of RNA (Supplementary Table 9) was measured in RNA buffer (100 mM KCl, 10 mM NaCl, 1 mM MgCl₂, 50 mM HEPES, pH 8.0) using time-correlated single photon counting. A PicoQuant FluoTime 100 fluorescence spectrometer and PicoQuant Picosecond Pulsed Diode Laser Heads with wavelengths 561 nm (LDH-D-TA-560) and 640 nm (LDH-P-C-640B) were used. Data were iteratively deconvoluted from the Instrument Response Function with one to three exponential decay functions, and the intensity weighted average lifetime values are reported.

Photobleaching measurements. Cbl-fluorophore probes and RNA were mixed, 3–4× of microscope immersion oil (Olympus immersion oil type-F) was added and the solution was emulsified to generate droplets. Samples were prepared in RNA buffer for Cbl-fluorophore samples (100 mM KCl, 10 mM NaCl, 1 mM MgCl₂, and 50 mM HEPES, pH 8.0) and in Broccoli buffer (40 mM HEPES pH 7.4, 100 mM KCl, and 1 mM MgCl₂) for the DFHBI-1T/Broccoli sample. The droplets were sandwiched between a glass slide and a coverslip. The sample was placed on the sample stage of a Nikon Ti-E HCA wide-field fluorescence microscope with the coverslip facing a 20× objective lens. All samples were continuously illuminated throughout the experiment at the irradiance reported in Supplementary Table 10. We assessed photostability by fixing the excitation rate, i.e., the number of absorbed excitation photons were the same for the Cbl-fluorophore/RNA samples and the DFHBI-1T/Broccoli sample. The high irradiance for the DFHBI-1T/Broccoli sample is a result of its low extinction coefficient. Images were acquired every 50 ms for DFHBI-1T/Broccoli and every 250 ms for others for 3 s, then every second for 47 s or longer, and the exposure time of each image was 15 ms for DFHBI-1T/Broccoli and 40 ms for others. A total of 6 to 15 droplets were analyzed for each sample.

In vitro fluorescence measurements. The concentration of Cbl-fluorophore probes, free fluorophores and free Cbl was determined using extinction coefficients listed in Supplementary Table 11. All in vitro experiments were conducted in RNA buffer (100 mM KCl, 10 mM NaCl, 1 mM MgCl₂, and 50 mM HEPES, pH 8.0). For the Cbl-fluorophore probes, the extinction coefficient of the fluorophores was used to determine the concentration. The shape of the absorption spectra did not change significantly for the conjugated probes compared to the sum of spectra for free fluorophores and free Cbl (Supplementary Fig. 32). The fluorescence intensity of each probe was measured with or without RNA as technical triplicates in a Tecan

Safire II fluorescence plate. The concentration of the probe was 0.25 μM or 0.5 μM and the RNA concentration was at least 5 μM, significantly above the dissociation constant (K_D) of the RNAs tested^{25,52}. Samples were incubated for at least 20 min at room temperature in the dark to allow Cbl-binding of the RNA before data collection. The excitation wavelength for each probe is listed in Supplementary Table 11 and the emission spectrum was collected in 1-nm increments for the range listed in Supplementary Table 11. Spectra were buffer subtracted, integrated and normalized to the signal of the free fluorophore at the same concentration.

Isothermal titration calorimetry (ITC). ITC experiments were performed using protocols previously established and described^{25,52}. Briefly, the RNA was dialyzed overnight at 4 °C into RNA buffer (100 mM KCl, 10 mM NaCl, 1 mM MgCl₂, 50 mM HEPES, pH 8.0) using 6,000–8,000 Da molecular weight cutoff dialysis tubing (Spectra/Por). The dialysis buffer was used to dissolve Cbl and Cbl-5× PEG-ATTO590 and to dilute RNA to the desired concentration. Titrations were performed at 25 °C using a MicroCal ITC₂₀₀ microcalorimeter (GE Healthcare), and data were fit using the Origin software suite as previously described⁵³.

Estimation of theoretical photophysical properties and distances in probes. The overlap integral $J(\lambda)$ of each fluorophore with Cbl absorbance was calculated from equation (1)⁵⁴:

$$J(\lambda) = \int_0^{\infty} F_D(\lambda) \epsilon_A(\lambda) \lambda^4 d\lambda \quad (1)$$

where F_D is the emission spectrum of the fluorophore normalized to unity and ϵ_A is the extinction coefficient of the acceptor (Cbl) in M⁻¹ cm⁻¹ using a MATLAB script [a|e - UV-Vis-IR Spectral Software 1.2, FluorTools, www.fluortools.com]. Fluorescence was recorded with a PTI-fluorimeter (1-nm steps, 1-s integration time, 2-nm slits for the excitation and 4-nm slits for detector). Cbl absorbance and fluorophore emission spectra (Supplementary Fig. 6) were converted in units of M⁻¹ cm⁻¹ (for absorbance of Cbl) and to unity (for emission of fluorophores) to calculate $J(\lambda)$. The Förster distance R_0 was calculated from equation (2)⁵⁴

$$R_0 = 0.211 (\kappa^2 n^{-4} Q_D J(\lambda))^{1/6} \quad (2)$$

where κ^2 is a factor describing the relative orientations of the transition dipoles and was assumed as $\kappa^2 = 2/3$ (ref. ⁵⁰); the refractive index n was assumed to be 1.4 for aqueous solutions. The quantum yield Q of each donor fluorophore is available from the manufactures (Supplementary Table 8).

The maximal distance between quencher and fluorophore in each probe was estimated as the length of the chemical linker (Supplementary Table 3) plus the distance between the 5' hydroxyl moiety of Cbl (where the linker is attached) and the corrin ring in the structure of Cbl²⁵, assuming that this region of Cbl harbors quenching properties. The distance between the 5'-hydroxyl moiety and the corrin ring was estimated to be 9 Å from the Cbl crystal structure²⁵. This distance was added to each linker lengths, resulting in the distances listed in Supplementary Table 5.

Construction of plasmids for mammalian expression of RNA tag variants.

Plasmids to produce RNA tags in mammalian cells were constructed by standard molecular cloning techniques (see Supplementary Fig. 11 for an overview and Supplementary Table 2 for RNA sequences). To construct mRNA fusions, the commercially available vector *pmCherry-C1* (Clontech) with a CMV promoter was used as a starting point. A *NheI* restriction site was introduced immediately following the stop codon by site-directed mutagenesis. The sequence of *mCherry* was then replaced with the *ACTB* sequence after PCR amplification of the insert from an existing plasmid (sequence was verified to be identical with *Homo sapiens* β-actin (ACTB), NCBI Reference Sequence NM_001101.4) with flanking *NheI* restriction sites. RNA tags were inserted between the stop codon and the poly(A) site using existing *KpnI* and *BamHI* restriction sites. Inserts encoding RNA tags were purchased as g-blocks or ultramers with restriction site overhangs from IDT. Sequences for RNA tags are summarized in Supplementary Table 2, and the published tRNA scaffold sequence¹⁷ was used. The monomeric RNA tag was introduced by ligating a purchased insert into the plasmid with *KpnI/BamHI* restriction sites resulting in ACTB-(A)1×. Additional copies were introduced sequentially, whereby the second and third copies were encoded on a g-block with *KpnI/KpnI* and *BamHI/BamHI* restriction sites, respectively, resulting in ACTB-(A)2× and ACTB-(A)3×. ACTB-(A)4× was the result of the third ligation step, in which colonies were screened for insertion of more than one copy of A. ACTB-(A)_n4× was constructed using the same strategy.

The 2×dBroccoli sequence²¹ to generate ACTB-2×dBroccoli and 1× and 2× copies of MS2 stem-loop (SL) sequences were purchased as a g-block with *KpnI* and *BamHI* overhangs and ligated downstream of the *ACTB* sequence as described for the riboswitch tag. The 4× MS2 SL sequence was generated by ligating a second 2× MS2 SL g-block sequence with *KpnI* restriction sites on both ends in the ACTB-(MS2-SL)2× plasmid. The 24×MS2 SL tag was built by first replacing the RNA tag downstream of *ACTB* with a short g-block sequence consisting of *NotI* and *PmeI*

sites using flanking *KpnI* and *BamHI* sites. Plasmid ACTB-(MS2-SL)24 \times was produced by cutting the 24 \times MS2-SL repeat from plasmid PGK1-24 \times MS2-SL⁹ with *NotI* and *PmeI* sites and ligating it downstream of the ACTB sequence via *NotI* and *PmeI* sites. Plasmids pAV5S-F30-2 \times dBroccoli and pAVU6+27-F30-2 \times dBroccoli³⁴ were gifts from S. Jaffrey (Addgene plasmid #66845 and #66842).

The existing plasmid pU1(human)³⁵ was modified to add the sequence of the RNA tag A_T immediately following the first 11 nucleotides of U1, analogous to previous U1 snRNA fusions⁴⁷. The parent plasmid was digested with two existing unique restriction sites (*BglII* is upstream of the U1 coding sequence and *PstI* is in the 3' region of the U1 coding sequence). An insert that contains the sequence for A_T and the surrounding U1 coding sequence including both restriction sites was purchased as a g-block from IDT and ligated, resulting in A_T -U1. All plasmids were verified by sequencing.

Cell culture and cell lines. U2-OS cells⁵⁶, HeLa cells and HEK 293 T cells (both purchased from ATCC) were maintained in Dulbecco's modified eagle medium (DMEM, Gibco) supplemented with 10% FBS (Gibco) at 37°C/5% CO₂. To generate a U2-OS cell line that stably produces GFP-G3BP1, the GFP-G3BP1 coding sequence was PCR amplified from a pGFP-C1-based vector with *EcoRI* and *NotI* overhangs and ligated into a Piggybac Dual Promoter plasmid that includes a puromycin resistance cassette for selection (System Biosciences, catalog #PB510B-1), resulting in plasmid pGFP-G3BP1-Piggybac. U2-OS cells were chemically transfected with pGFP-G3BP1-Piggybac and Super PiggyBac Transposase expression vector (System Biosciences, catalog #PB220PA-1) using *TransIT* according to manufacturer recommendations (Mirus). After selection with 1 μ g/mL puromycin, U2-OS cells stably producing GFP-G3BP1 were FACS enriched for the brightest 30% of GFP-fluorescent cells.

To generate a U2-OS cell line that stably produces MS2-GFP, the MS2-GFP sequence was PCR amplified from plasmid pMS2-GFP (a gift from R. Singer, Addgene plasmid #27121) with *XbaI* and *NotI* overhangs, ligated into the Piggybac Dual Promoter plasmid, transfected in U2-OS cells with a Halo-G3BP1 genetic background, and selected and FACS enriched as described above.

Introduction of an N-terminal 3 \times FLAG-HALO epitope tag to the endogenous G3BP1 protein was performed as previously described³⁷ with the following modifications (Supplementary Fig. 33). First, two single-strand breaks were generated flanking the translational start site of G3BP1 with dual CRISPR-Cas9 nickases (D10A) in U2-OS cells. Correct targeting of CRISPR guides was confirmed by T7 endonuclease assay (NEB). Cells were selected with puromycin to enrich for edited cells containing the sequence for the tags and the LoxP-flanked, SV40-driven puromycin expression cassette. Removal of the puromycin expression cassette and in frame expression of 3 \times Flag-HALO was achieved by transient transfection of the eGFP-Cre plasmid. Transiently transfected cells were enriched by FACS. Correctly edited cells were confirmed by PCR, western blot and immunofluorescence using standard protocols.

Halo-staining. Halo dyes JF585, SiR594 and JF646 were gifts from L. Lavis. Cells were incubated with 1 μ M Halo dye in media containing DMEM/5% FBS for 20 min at 37°C/5% CO₂. Unbound dye was washed out by replacing the media first with PBS and then with DMEM/5%FBS media before further treatment was performed (arsenite treatment, bead loading, see below).

Bead loading. Cells were seeded in home-made imaging dishes (35-mm diameter) with a ~10 mm center hole covered by cover glass (No. 1.5, VWR). Culture media was removed, and the Cbl-fluorophore probe (3 μ L of a 50 μ M stock in PBS for U-body imaging in HeLa cells, 3 μ L of a 0.5 μ M stock in PBS for mRNA imaging via Cbl-Cy5 in U2-OS cells and 3 μ L of a 5 μ M stock in PBS for mRNA imaging via Cbl-4 \times Gly-ATTO 590 in U2-OS cells) was added directly on the cells. Microbeads were sprinkled onto the cells, and the dye was loaded as described previously^{16–38}. Culture media was added immediately, supplemented with arsenite for stress granules imaging (see below).

Stress granule (SG) assay. U2-OS cells producing GFP-G3BP1 or Halo-G3BP1 were seeded at 0.25 \times 10⁶ cells in imaging dishes. One day after seeding, cells were chemically transfected with 2 μ g plasmid DNA (1 μ g of the ACTB-RNA tag fusion mixed with 1 μ g of the transfection marker pNLS-TagBFP) using the *TransIT* transfection system following manufacturer recommendations (Mirus). On the next day, cells were stained with Halo dye and loaded with the Cbl-fluorophore probe as described above. Media added after bead loading contained 0.5 mM sodium arsenite, and cells were incubated at 37°C/5% CO₂ for 30–45 min to induce stress granules. Cells were rinsed once in PBS, and FluoroBrite media (Gibco) supplemented with 0.5 mM sodium arsenite was used for live cell imaging. For correlative imaging, cells were first imaged live, followed by fixation and FISH/immunofluorescence imaging of the same cells and the following modifications were made: gridded imaging dishes (MatTek) were coated with 1 μ g/mL fibronectin (Sigma) for 4 h; following one rinse with full media, plasmid ACTB-(A_T)₄ \times was used and 3 μ L of 50 μ M Cbl-5 \times PEG-ATTO 590 was bead loaded.

U-body assay. HeLa cells were seeded at 0.1–0.15 \times 10⁶ cells per imaging dish. One day after seeding, cells were chemically transfected with 1 μ g plasmid DNA

(A_T -U1) using *TransIT* following manufacturer recommendations (Mirus). For experiments with marker proteins, 0.25 μ g of GFP-SMN⁵⁸ (a gift from G. Matera, Addgene plasmid #37057) was co-transfected. For colocalization experiments with coilin, 0.5 μ g pEGFP-coilin⁵⁹ (a gift from G. Matera, Addgene plasmid #36906) was transfected with or without co-transfection of 0.5 μ g plasmid DNA encoding A_T -U1. Imaging or fixation was performed the following day. For live cell imaging, cells were treated with 10 μ M thapsigargin for 3 h before the Cbl-fluorophore probe was bead loaded and imaged within 1 h after loading. For immunofluorescence or FISH analysis, cells were fixed 3–4 h after thapsigargin treatment.

Fluorescence microscopy and image analysis. Fluorescence microscopy was performed on a Nikon A1R Laser Scanning Confocal Microscope with a 100 \times oil objective (1.45 NA, Plan Apo I), a pixel size of 0.25 μ m and an integration time of 2.2 μ s unless otherwise noted below or in Supplementary Table 12. Images were acquired at 16-bit depth with Nikon Elements Software and processed in ImageJ2 using the Fiji plugin. All live images were acquired with an environment chamber at 37°C. Laser lines used were 405 nm (DAPI, for nuclear staining and NLS-TagBFP imaging), 488 nm (GFP, for GFP-tagged proteins and Broccoli-tagged mRNA), 561 nm (TRITC, for ATTO 590 in Cbl-fluorophore probes and Alexa 546, Alexa 594 and Alexa 568 in FISH probes and secondary antibodies and for Halo-dyes JF595 and SiR594) and 638 nm (Cy5, for Cy5 and Halo-dye JF646). Image acquisition settings for each experiment are listed in Supplementary Table 12.

For live imaging of Broccoli-tagged 5S and U6 RNA, published protocols were used²¹. Briefly, plasmids pAVU6+27-F30-2 \times dBroccoli and pAV5S-F30-2 \times dBroccoli²¹ were transfected in HEK 293 T cells and split into imaging dishes 48 h post-transfection. Twenty four hours later, DFHBI-1T was added at a final concentration of 40 μ M and cells were imaged under wide-field illumination conditions as recommended²¹ using a 60 \times oil objective and 250 ms exposure. No neutral density (ND) filters were used.

Immunofluorescence. Cells were fixed in 4% paraformaldehyde (EM grade, Electron Microscopy Sciences) for 10 min, rinsed three times in PBS and permeabilized for 10 min in PBS/0.2% Triton X-100 at room temperature, which was followed by three rinses in PBS. After blocking for 30 min at room temperature in PBS/5% FBS, slides were incubated with the primary antibody against DDX20 (mouse monoclonal; sc-57007, Santa Cruz Biotechnology; 1:200 dilution) or SMN (rabbit polyclonal; sc-15320, Santa Cruz Biotechnology; 1:200 dilution) in PBS/5% FBS at 4°C overnight. After three rinses in PBS, slides were incubated with the secondary antibody (1:1,000 dilution in both cases) and Hoechst nuclear dye (1:10,000 dilution) for 90 min at room temperature. The secondary antibody for DDX20 was a goat anti-mouse Alexa 594 antibody (A11005, Lot# 55579A, Invitrogen), and the secondary antibody for SMN was a donkey anti-rabbit Alexa 568 antibody (A10042, Lot# 1134929, Invitrogen). Slides were rinsed three times in PBS and once in water. If no FISH was performed subsequently, slides were mounted.

Fluorescence in situ hybridization (FISH). When no immunofluorescence was performed before FISH, cells were fixed in 4% paraformaldehyde and permeabilized in 0.2% Triton X-100 as described above. When FISH was performed after immunofluorescence, no additional permeabilization step was performed. Cells were dehydrated sequentially in 70%, 95% and 100% ethanol for 5 min each. After a 2-min drying step, cells were rehydrated in 2 \times SSC (1 \times SSC is 150 mM NaCl, 15 mM sodium citrate dihydrate, pH 7.0) and 50% formamide (molecular biology grade) for 5 min. Slides were prehydrated in prehybridization solution (50% formamide, 2 \times SSC, 0.5 mg/mL UltraPure Salmon sperm DNA (Thermo Fisher Scientific), 1 mg/mL UltraPure BSA (Thermo Fisher Scientific), 0.13 mg/mL *Escherichia coli* tRNA (Sigma-Aldrich), 1 mM Vanadyl ribonucleoside complexes solution (Sigma-Aldrich) and 100 mg/mL dextran sulfate in ultrapure water) for 30 min at 37°C. After prehybridization, samples were hybridized with the probe (Supplementary Table 13) in prehybridization solution overnight at 37°C. On the following day, samples were washed twice in 2 \times SSC/50% formamide for 30 min each. Slides were rinsed in PBS once and sealed.

Northern blotting. Production and processing of RNA fusion variants was assessed in HEK 293 T cells. Dishes were coated with 10 μ g/mL poly-L-lysine for 1 h and rinsed, and 2 \times 10⁶ cells were seeded per 10 cm dish. On the following day, 15 μ g plasmid DNA was transfected per dish using the *TransIT* (Mirus) chemical transfection system according to manufacturer recommendations. Cells were harvested 48 h after transfection, and total RNA was extracted using the RNeasy (Qiagen) kit according to manufacturer recommendations. The final RNA concentration was typically 500–1,000 ng/ μ L.

All solutions for gel electrophoresis and northern blotting were made in diethyl pyrocarbonate (DEPC)-treated and autoclaved water. 10 μ g total RNA per lane were dried in a SpeedVac, and the RNA was brought up in 15 μ L of RNA sample buffer (50% v/v formamide, 6.3% v/v formaldehyde, 0.2 M MOPS, 50 mM sodium acetate pH 5.2, 10 mM EDTA pH 8.0) plus 2 μ L of RNA loading buffer (50% glycerol, 1 mM EDTA pH 8.0, 0.4% bromophenol blue, 1 mg/mL ethidium bromide). Samples were heated at 65°C for 5 min and loaded on a 1% agarose/formaldehyde gel (50 mM sodium acetate pH 5.2, 10 mM EDTA pH 8.0, 1% w/v agarose, 6.3% formaldehyde). 10 μ L of a Low Range ssRNA Ladder (New England

BioLabs) was loaded as well. The gel was run in running buffer (50 mM sodium acetate pH 5.2, 10 mM EDTA pH 8.0, 6.3% formaldehyde) at 60 V for 2.5 h. To assess the quality of the isolated RNA, the gel was then stained with ethidium bromide (10 μ L of 10 mg/mL ethidium bromide in 400 mL running buffer).

After destaining in water for 5 min, the RNA was transferred to a nylon membrane (Amersham Hybond-N⁺, GE Healthcare) using standard procedures. The RNA was crosslinked to the membrane by exposure to UV light, washed in 0.1 \times SSC and 0.1% sodium dodecyl sulfate (SDS) at 65 °C for 1 h and prehybridized for 1 h in hybridization solution (6 \times SSC, 10 \times Denhardt's solution (Life Technologies), 0.1% SDS) at 42 °C. The membrane was then incubated with hybridization solution supplemented with the radioactive, labeled probe overnight at 42 °C. After 3 wash steps for 5 min at room temperature in washing solution (6 \times SSC, 0.1% SDS) and an additional wash step at 48 °C for 20 min, the membrane was dried and exposed overnight. Exposure and visualization of the ³²P signal was done using the Phosphor Screen and Cassette System from GE Healthcare. The membrane was stripped to subsequently hybridize with another probe.

Radioactive probes (sequence listed in Supplementary Fig. 12c) were produced as follows. From a 100 μ M stock of DNA probes, 2 μ L were mixed with 2 μ L ³²P-ATP, 2 μ L T4 Polynucleotide Kinase (PNK) (NEB), 2 μ L of 10 \times T4 PNK buffer (NEB) in water and incubated at 37 °C for at least 1 h. The DNA was then passed over a G-25 column (GE Healthcare) according to manufacturer recommendations to remove unincorporated ATP.

Reporting Summary. Further information on experimental design is available in the Nature Research Reporting Summary linked to this article.

Data availability. The datasets generated during and/or analyzed during the current study are available from the corresponding author on reasonable request.

References

51. Edwards, A. L., Garst, A. D. & Batey, R. T. Determining structures of RNA aptamers and riboswitches by X-ray crystallography. *Methods Mol. Biol.* **535**, 135–163 (2009).
52. Polaski, J. T., Holmstrom, E. D., Nesbitt, D. J. & Batey, R. T. Mechanistic insights into cofactor-dependent coupling of RNA folding and mRNA transcription/translation by a cobalamin riboswitch. *Cell Rep.* **15**, 1100–1110 (2016).
53. Gilbert, S. D. & Batey, R. T. Monitoring RNA-ligand interactions using isothermal titration calorimetry. *Methods Mol. Biol.* **540**, 97–114 (2009).
54. Lakowicz, J. R. Quenching of Fluorescence. in *Principles of Fluorescence Spectroscopy* 277–330 (Springer, 2006).
55. Beckley, S. A. et al. Reduction of target gene expression by a modified U1 snRNA. *Mol. Cell. Biol.* **21**, 2815–2825 (2001).
56. Wheeler, J. R., Matheny, T., Jain, S., Abrisch, R. & Parker, R. Distinct stages in stress granule assembly and disassembly. *eLife* **5**, 1–25 (2016).
57. Xi, L., Schmidt, J. C., Zaug, A. J., Ascarrunz, D. R. & Cech, T. R. A novel two-step genome editing strategy with CRISPR-Cas9 provides new insights into telomerase action and TERT gene expression. *Genome Biol.* **16**, 231 (2015).
58. Shpargel, K. B. & Matera, A. G. Gemin proteins are required for efficient assembly of Sm-class ribonucleoproteins. *Proc. Natl Acad. Sci. USA* **102**, 17372–17377 (2005).
59. Shpargel, K. B., Ospina, J. K., Tucker, K. E., Matera, A. G. & Hebert, M. D. Control of Cajal body number is mediated by the coilin C-terminus. *J. Cell Sci.* **116**, 303–312 (2003).

Reporting Summary

Nature Research wishes to improve the reproducibility of the work that we publish. This form provides structure for consistency and transparency in reporting. For further information on Nature Research policies, see [Authors & Referees](#) and the [Editorial Policy Checklist](#).

Statistical parameters

When statistical analyses are reported, confirm that the following items are present in the relevant location (e.g. figure legend, table legend, main text, or Methods section).

n/a Confirmed

- The exact sample size (n) for each experimental group/condition, given as a discrete number and unit of measurement
- An indication of whether measurements were taken from distinct samples or whether the same sample was measured repeatedly
- The statistical test(s) used AND whether they are one- or two-sided
Only common tests should be described solely by name; describe more complex techniques in the Methods section.
- A description of all covariates tested
- A description of any assumptions or corrections, such as tests of normality and adjustment for multiple comparisons
- A full description of the statistics including central tendency (e.g. means) or other basic estimates (e.g. regression coefficient) AND variation (e.g. standard deviation) or associated estimates of uncertainty (e.g. confidence intervals)
- For null hypothesis testing, the test statistic (e.g. F , t , r) with confidence intervals, effect sizes, degrees of freedom and P value noted
Give P values as exact values whenever suitable.
- For Bayesian analysis, information on the choice of priors and Markov chain Monte Carlo settings
- For hierarchical and complex designs, identification of the appropriate level for tests and full reporting of outcomes
- Estimates of effect sizes (e.g. Cohen's d , Pearson's r), indicating how they were calculated
- Clearly defined error bars
State explicitly what error bars represent (e.g. SD, SE, CI)

Our web collection on [statistics for biologists](#) may be useful.

Software and code

Policy information about [availability of computer code](#)

Data collection

Microscopy images were acquired with Nikon Elements Software.

Data analysis

Analysis of Isothermal titration calorimetry was done in Origin 5.0. Image display and line trace analysis for fluorescence analysis in stress granules was done in ImageJ2 with the Fiji plugin suite. Statistical ANOVA analysis was done in KaleidaGraph version 4.02. The One Way ANOVA test in KaleidaGraph was used with the Tukey's All Pairs Comparison option. In vitro fluorescence measurements were analyzed in Microsoft Excel 2013 to calculate mean and standard deviation.

For manuscripts utilizing custom algorithms or software that are central to the research but not yet described in published literature, software must be made available to editors/reviewers upon request. We strongly encourage code deposition in a community repository (e.g. GitHub). See the Nature Research [guidelines for submitting code & software](#) for further information.

Data

Policy information about [availability of data](#)

All manuscripts must include a [data availability statement](#). This statement should provide the following information, where applicable:

- Accession codes, unique identifiers, or web links for publicly available datasets
- A list of figures that have associated raw data
- A description of any restrictions on data availability

The datasets generated during and/or analysed during the current study are available from the corresponding author on reasonable request.

Field-specific reporting

Please select the best fit for your research. If you are not sure, read the appropriate sections before making your selection.

Life sciences Behavioural & social sciences Ecological, evolutionary & environmental sciences

For a reference copy of the document with all sections, see [nature.com/authors/policies/ReportingSummary-flat.pdf](https://www.nature.com/authors/policies/ReportingSummary-flat.pdf)

Life sciences study design

All studies must disclose on these points even when the disclosure is negative.

Sample size	<p>No statistical method was used to predetermine sample size. The following considerations were used to determine that the sample sizes used for each experiment are sufficient.</p> <p>In vitro biochemical measurements (fluorescence measurements, ITC) were repeated 3 times or more (as indicated in figure legends) for calculation of mean +/- STDEV. The STDEV was typically below 10% for fluorescence measurements, and we concluded that these measurements are sufficient to determine trends of fluorescence quenching and de-quenching for the study. Three measurements were deemed reliable to compare the affinity between Cbl and a representative probe.</p> <p>The Northern blot (Supplementary Fig. 12) was reproducible for two independent experiments. This was deemed sufficient, as the processing phenotype was robust and easily detected.</p> <p>For control experiments involving fixed cells (immunofluorescence and FISH), a large subset of experiments are reproduced from known literature localization patterns as controls for the live cell experiments (as indicated in the main text). For example, beta actin localization to GFP-G3BP1-labelled SGs was demonstrated by diverse methods in different laboratories by different groups. Furthermore, phenotypes were analyzed by orthogonal methods. For example, U-body formation was confirmed via SMN and DDX20 localization; tagged U1 localization to U-bodies was confirmed by testing co-localization to both orthogonal marker proteins. Together, it was deemed sufficient to repeat these experiments on fixed cells once or twice for each specific condition (as indicated in figure legends), and the total number of cells interrogated is noted in each figure legend.</p> <p>Control live fluorescence experiments to determine uptake by bead loading in different cell lines (Supplementary Fig. 13) was done once or twice for the exact conditions shown, and ~50 or more cells were interrogated (as detailed in the figure legend). This was deemed sufficient, as similar localization patterns were observed in non-transfected controls throughout the study.</p> <p>For live cell imaging to assess mRNA colocalization to SGs, at least 2 separate experiments were performed for each condition. Timing of live cell imaging was critical such that cell death upon prolonged arsenite treatment does not interfere with data analysis. With these constraints, >50 stress granules were analyzed per condition. The analysis of these measurements revealed statistical significance. We concluded that our data is robust because we observed consistent trends for imaging with probes of two different colors and for tagging with monomers versus multimers of our RNA tag. For live cell imaging of U-bodies (Fig. 5), we performed four separate experiments and analyzed hundreds of cells per condition. We concluded that these numbers were sufficient as we observed a statistically significant differences.</p>
Data exclusions	<p>For the U-body assay, thapsigargin treatment was done for 3 hours for all experiments reported, but for initial pilot experiments the thapsigargin treatment was longer and more variable (>4 hours). These data were excluded as U-body formation is likely time-dependent and this variable should not be altered whenever possible.</p>
Replication	<p>All attempts at replication were successful, and we have indicated in each figure legend how many times each experiment was independently repeated.</p>
Randomization	<p>Randomization of samples in groups is not relevant to this study as no animal or clinical work was performed.</p>
Blinding	<p>In vitro fluorescence measurements were not blinded as automated analysis on the plate reader on fluorimeter is unbiased. For live cell imaging, blinding was not possible for the following reasons. Quantification of RNA localization to stress granules (Supplementary Figure 18) was developed while data sets were collected.</p> <p>The U-body analysis was not blinded, as several of the transfected datasets were initially collected with the goal to perform FISH on the same fixed cells. While this correlative imaging of live and fixed cells failed for technical reasons, the live cell images were useable for the analysis presented in Fig. 5b. Cells used for the analysis in Fig. 5b were imaged as 'large images' (such as 8x8 scans) to achieve an objective set of cells from the population without 'cherry picking' cells.</p> <p>Immunofluorescence and FISH experiments were not blinded as most experiments are control experiments to validate the live experiments and these fixed immunofluorescence / FISH experiments reproduce localization patterns shown in the literature.</p>

Reporting for specific materials, systems and methods

Materials & experimental systems

n/a	Involvement	Material
<input type="checkbox"/>	<input checked="" type="checkbox"/>	Unique biological materials
<input type="checkbox"/>	<input checked="" type="checkbox"/>	Antibodies
<input type="checkbox"/>	<input checked="" type="checkbox"/>	Eukaryotic cell lines
<input checked="" type="checkbox"/>	<input type="checkbox"/>	Palaeontology
<input checked="" type="checkbox"/>	<input type="checkbox"/>	Animals and other organisms
<input checked="" type="checkbox"/>	<input type="checkbox"/>	Human research participants

Methods

n/a	Involvement	Method
<input checked="" type="checkbox"/>	<input type="checkbox"/>	ChIP-seq
<input checked="" type="checkbox"/>	<input type="checkbox"/>	Flow cytometry
<input checked="" type="checkbox"/>	<input type="checkbox"/>	MRI-based neuroimaging

Unique biological materials

Policy information about [availability of materials](#)

Obtaining unique materials

We will deposit plasmids generated in this study (Supplementary Fig. 11) at Addgene upon acceptance of this manuscript for publication. Several synthetic Cobalamin-fluorophore probes were developed in this study. While we may be able to provide small quantities of these materials if requested, we would like to point out that synthesis produced limited quantities of these materials. Detailed methods on how to synthesize these probes are provided in the Supplementary Note.

Antibodies

Antibodies used

Two primary antibodies were used:
 (1) DDX20 antibody: Gemin3 (12H12): sc-57007, Lot# E0614, Santa Cruz Biotechnology, mouse monoclonal antibody raised against amino acids 368-548 of Gemin3 of human origin, 1:1,000 dilution.
 (2) SMN antibody: SMN (H-195): sc-15320, Lot# B1512, Santa Cruz Biotechnology, rabbit polyclonal antibody raised against amino acids 1-195 mapping at the N-terminus of SMN of human origin.
 Two secondary antibodies were used. Goat anti-mouse Alexa 594 antibody: A11005, Lot# 55579A, Invitrogen. Donkey anti-rabbit Alexa 568 antibody: A10042, Lot# 1134929, Invitrogen, 1:1,000 dilution.

Validation

The DDX20 antibody was validated to detect U-bodies (cytosolic puncta upon treatment with various stimuli including thapsigargin) in HeLa cells by Tsaliki J, Tattoli I, Ling A, Sorbara MT, Croitoru DO, Philpott DJ, Girardin SE, JBC, 2015, doi: 10.1074/jbc.M115.659466). This phenotype was reproduced in the present study for validation (Supplementary Fig. 28). Tsaliki et al validated that a SMN antibody detects U-bodies (cytosolic puncta upon treatment with stimuli) in HeLa cells using a home-made SMN antibody. The commercial SMN antibody used in the present study was validated to detect U-bodies in HeLa cells, resulting in puncta comparable with literature patterns (Supplementary Fig. 28).

Eukaryotic cell lines

Policy information about [cell lines](#)

Cell line source(s)

HeLa and 293T cells were purchased from ATCC and only used for up to 12 passages upon receipt. U2-OS cells were received from Roy Parker and described previously (Wheeler JR, Matheny T, Jain S, Abrisch R, Parker R, Elife. 2016, doi: 10.7554/eLife.18413.). The U2-OS cell line with genomic Halo-G3BP1 was generated in this study (see methods section for details and Supplementary Figure 33).

Authentication

HeLa and 293T cells were purchased from ATCC and not further authenticated, as they were only used for up to 12 passages upon receipt from ATCC. U2-OS cells were received from Professor Roy Parker (Wheeler JR, Matheny T, Jain S, Abrisch R, Parker R, Elife. 2016, doi: 10.7554/eLife.18413.). U2OS cells were also purchased from ATCC and not further authenticated. Validation of the U2-OS cell line with genomic Halo-G3BP1 generated in this study is presented in Supplementary Fig. 33. Correctly edited cells were confirmed by PCR, Western blot and immunofluorescence using standard protocols.

Mycoplasma contamination

All eukaryotic cell lines (HeLa, 293T, U2-OS) were regularly (at least bi-yearly) tested for mycoplasma contamination by staff at the in-house Cell Culture Core Facility at the BioFrontiers Institute. No mycoplasma contaminations were detected for all three cell lines or other cell lines in the Palmer laboratory throughout the duration of the study.

Commonly misidentified lines (See [ICLAC](#) register)

No commonly misidentified cell lines were used.